Complex nonlinear behavior in optically excited nematic liquid crystals

G. Demeter*
Physikalisches Institut der Universität Bayreuth, D-95440 Bayreuth, Germany
(Received 7 December 1999)

We present a study of the passage of a monochromatic, linearly polarized cw laser beam through a cell of homeotropically aligned nematic liquid crystal at a slightly oblique angle. The light is polarized perpendicular to the plane of incidence. Experiments in this geometry have revealed the existence of complex, time-dependent dynamics of the director motion. We present a model for the director dynamics derived from the basic equations that shows both periodic and chaotic behavior at different light intensities as observed in the experiments. The model we derive exhibits a variety of complex behaviors, among them an uncommon route to chaos via gluing bifurcations that has not yet been observed in any real physical system.

PACS number(s): 42.70.Df, 05.45.Ac, 42.65.Sf

I. INTRODUCTION

Liquid crystals (LCs) are known to produce a great variety of interesting optic phenomena, in particular those associated with the so-called light-induced director reorientation. LCs are optically anisotropic materials, and their local optical properties (the direction of the optical axis) are determined by the orientation of the director. This, on the other hand, is influenced by the electric field of a light wave. Thus an intense light wave can alter the optical properties of the material it propagates through. This leads to a rich variety of nonlinear optical responses of the LC cell (see [1,2]).

In some configurations, a steady continuous wave (cw) illumination of the liquid crystal produces a persistent time-dependent behavior of the director. An example is the case of circularly or elliptically polarized light incident at right angles to a cell of homeotropically aligned LC. Angular momentum exchange between the light field and the LC causes precession and nutation of the director [3].

Another, even more interesting configuration is that of a linearly polarized light wave incident upon a cell of homeotropically aligned nematic LC at a small angle s_0. The direction of polarization is perpendicular to the plane of incidence in this case [see Fig. 1(a)]. Early experiments with this arrangement revealed periodic and irregular motion of the director [4,5]. There has been considerable experimental effort to explore the properties of the irregular regime recently [6–9]. Observations show that the initial oscillations grow more complex as the intensity of the incident laser beam increases, eventually turning chaotic. While attempts at deriving a model for this complex behavior have begun [8,10], a proper theory derived from the basic equations that reproduces this chaotic behavior has not yet been developed.

In this paper we report on the derivation of a set of ordinary differential equations (ODEs) for the motion of the director from the fundamental equations for LCs and electromagnetic waves. We solve these equations with a computer and show that they indeed give rise to complex and chaotic dynamics in good agreement with existing experimental observations. Thus they represent a good starting point for understanding some of these complex phenomena. The model is found to exhibit various routes to chaos, among them a rather distinct one through a series of gluing bifurcations [11–13]. To our knowledge, this route to chaos has never been experimentally observed in any real physical system. It is also suggested that the experimental system can be generalized slightly by using an additional static electric or magnetic field to produce an even larger variety of nonlinear behavior. Since the control parameters of the problem (the intensity of the laser, the angle of incidence, and the amplitude of the additional static field) can be controlled accurately and easily, further study of this system should be interesting from the point of view of basic chaos theory.

This paper is organized as follows. In the second section we summarize the derivation of our equations and the most important assumptions made. We sketch the general form of the equations obtained, the detailed calculations being presented in the Appendix. We show that the simplest model we can construct to describe the observed phenomena is a three-variable model. In the third section we present results of the numerical solution of these equations and compare the results with published experimental findings. We show that the model exhibits complex nonlinear behavior and various routes to chaos, among them a rather distinct route that has not yet been observed in an experimental system. In the fourth section we show that refined versions of our model using more variables also possess the basic properties that make this particular scenario of transition to chaos possible.

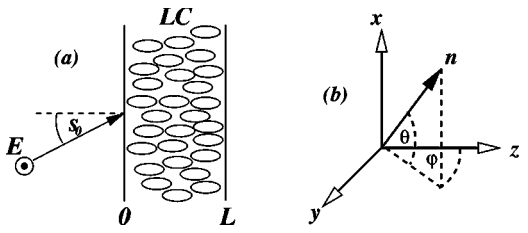

FIG. 1. (a) Geometry of the setup: a slightly oblique ordinary wave incident upon a cell of nematic LC with homeotropic orientation. (b) Definition of the angles describing the orientation of the director.

*On leave from the Research Institute for Particle and Nuclear Physics of the Hungarian Academy of Sciences, Budapest, Hungary.

Finally, we generalize our model slightly with the inclusion of additional static electric and magnetic fields and discuss the advantages of studying such a sytem. A short account of some of the results presented here has been published in [14].

II. MATHEMATICAL MODEL

We consider the scenario depicted in Fig. 1(a), with a linearly polarized plane wave incident upon a cell of homeotropically aligned nematic LC at a small angle s_0. The direction of polarization is assumed to be perpendicular to the plane of incidence, i.e., the incident wave is an ordinary wave. We assume strong anchoring of the nematic at the boundaries of the cell. We describe the time- and space-dependent orientation of the director $\mathbf{n}(\mathbf{r},t)$ using two angles $\theta(\mathbf{r},t)$ and $\varphi(\mathbf{r},t)$ [see Fig. 1(b)] and seek dynamical equations for their evolution. These equations will include terms that describe the torque exerted on the director by the electric field of the light wave as well as the elastic stresses that arise in the LC as a response to deformations of the homogeneous alignment. The main difficulty is that the electric field $\mathbf{E}(\mathbf{r},t)$ must be obtained from Maxwell's wave equations with the $\mathbf{r}$-dependent dielectric tensor given by $\epsilon_{ij}=\varepsilon_\perp\delta_{ij}+\varepsilon_a n_i n_j$ (here $\varepsilon_\perp$ is the dielectric permittivity perpendicular to $\mathbf{n}$, $\varepsilon_a=\varepsilon_\parallel-\varepsilon_\perp$ the dielectric anisotropy).

To simplify the problem, we assume that (a) the orientation of the director depends on the z coordinate only and (b) the angles are small ($|\theta|,|\varphi|\ll 1$). This latter assumption allows us to expand all expressions as power series in these angles and drop all terms of higher than third order. It also allows us to use perturbation theory when calculating the electric field corresponding to the reoriented state of the LC. To obtain a set of ODE's for the time evolution of the angles, we write them as a sum of sine functions that satisfy the boundary conditions $\varphi(z,t)=\Sigma_n A_n(t)\sin(n\pi z/L)$, $\theta(z,t)=\Sigma_n B_n(t)\sin(n\pi z/L)$ (L is the thickness of the cell), and project the original system of equations on these modes. After truncating this system we have a finite number of amplitudes $(A_1,\ldots,A_n,B_1,\ldots,B_m)$ and a set of coupled, first order, nonlinear ODE's for these variables that contain terms up to third order. Their general form is

$$\tau\dot{A}_i=\sum_j L^A_{ij}A_j+\sum_{j,k} P^A_{ijk}A_jB_k+\sum_{\substack{j,k,l\\ k\leqslant l}} Q^A_{ijkl}A_jB_kB_l + \sum_{j\leqslant k\leqslant l} R^A_{ijkl}A_jA_kA_l,$$

$$\tau\dot{B}_i=\sum_j L^B_{ij}B_j+\sum_{j\leqslant k} P^B_{ijk}A_jA_k+\sum_{\substack{j,k,l\\ k\leqslant l}} Q^B_{ijkl}B_jA_kA_l + \sum_{j\leqslant k\leqslant l} R^B_{ijkl}B_jB_kB_l,$$

where $\tau=\gamma L^2/\pi^2K_3$ is the characteristic time of the director motion (γ is the rotational viscosity of the LC and K_3 is the elastic constant of with respect to bend deformations; see [1,2]). The inversion symmetry with respect to the x-z plane implies that the equations must be invariant under the transformation $S:\{A_i\}\to\{-A_i\}$, so that only odd powers of the A_i's can appear in the first set of equations and only even powers in the second set. The linear coefficients L^A,L^B and the nonlinear ones P^A,Q^A,R^A,P^B,Q^B,R^B are functions of $s=s_0/\sqrt{\varepsilon_\perp}$ (the angle of refraction of an ordinary wave in the cell), $\varepsilon'_a=\varepsilon_a/\varepsilon_\perp$ (dielectric anisotropy parameter), the ratios of the Frank constants K_1/K_3, K_2/K_3, the intensity parameter ρ defined as

$$\rho=\frac{I}{I_F},\quad I_F=\frac{\pi^2}{L^2}\frac{c(\varepsilon_\perp+\varepsilon_a)K_3}{\varepsilon_a\sqrt{\varepsilon_\perp}}$$

[I is the laser intensity, I_F is the threshold intensity of the light-induced Fréedericksz transition (LIFT) for perpendicular incidence [1,2]], and the parameter κ:

$$\kappa=\frac{L}{\pi}\frac{s_0^2\varepsilon_a k_0}{2\sqrt{\varepsilon_\perp}(\varepsilon_\perp+\varepsilon_a)}$$

(k_0 is the wave number of the incident light in vacuum). $\kappa\pi$ is (to a very good approximation) the phase shift between an ordinary and an extraordinary wave (the latter is polarized in the plane of incidence) at $z=L$ in the case of undisturbed homeotropic alignment of the LC. The detailed derivation of the equations that yields the precise expressions for the various coefficients is presented in the Appendix.

To consider the number of modes we must keep to be able to describe the observed phenomena, we examine the linear terms of the equations. The general expressions for these terms in the limit $\kappa^2\ll 1$ when terms proportional to κ^4 can be omitted are

$$L^A_{mm}=-m^2+\rho+\frac{\kappa^2\rho}{m^2}[1+2(-1)^m],$$

$$L^A_{mn}=\frac{2(-1)^m\kappa^2\rho}{mn},\quad m\neq n, \tag{1}$$

$$L^B_{mn}=-m^2\delta_{mn}$$

(see the Appendix). This limit is sufficient for our purposes as by using parameters corresponding to the experimental setup of [6,7] (see [15]) we obtain $\kappa^2\approx 0.06$. One can see that in the absence of incident light ($\rho=0$) all the modes are damped proportionally to m^2. This is simply due to the elastic stress that a sinusoidal reorientation induces in the LC. A mode of higher order (i.e., shorter wavelength) induces greater stress. The incident light excites modes of φ (reorientation in the y direction—the direction of polarization) but not θ, so the B_i amplitudes are always linearly stable. The first mode to become unstable in the φ direction is the A_1 mode, and the threshold intensity (the intensity when the electric excitation overcomes the elastic damping) is $\rho_c=1+O(\kappa^2)$, only slightly increased by the nonzero angle of incidence. The coupling between the different φ modes induced by the electric field is also proportional to κ^2 so we anticipate that those modes that are very far from being linearly unstable are not excited significantly and can be neglected. The intensities we consider here lie in the region $\rho\approx 1$–2.5, so that only the A_1 mode becomes unstable and it is

sufficient to take the first two modes in the φ direction (A_1, A_2) and the first mode in the θ direction (B_1) to describe our system. The following two modes A_3, B_2 have a linear damping rate several times larger than these three in this intensity region. Since we need at least three variables to obtain chaotic behavior, this three-variable model with third order nonlinearities is also the simplest one that can be expected to exhibit the complex behavior observed in the experiments.

III. ROUTES TO CHAOS IN THE THREE-VARIABLE MODEL

A. Transition to chaos via gluing bifurcations

The equations obtained for the three-variable model can be solved numerically for various parameter values. We explored the behavior of the model using the light intensity ρ and the angle of incidence s_0 as control parameters. All other parameters were chosen to correspond to the setup used in the experiments [6,7] (see [15]).

First we discuss the case $s_0 = 7°$, which is the angle of incidence used in the experiments. At this angle, the basic state $(A_1 = A_2 = B_1 = 0)$ loses stability at $\rho_c \approx 1.065$. It becomes a saddle point and two symmetry degenerate off-origin fixed points are produced, which corresponds to a stationary reorientation of the LC (LIFT). The symmetry S is broken spontaneously. Not too far above ρ_c the amplitude A_1 dominates, which corresponds to a simple sinusoidal reorientation in the y direction. At higher intensities the nonlinear interaction between the modes becomes important, leading to the growth of A_2 and B_1.

The stationary reoriented state becomes unstable in a Hopf bifurcation at $\rho_0 \approx 1.71$ and two simple limit cycles appear in phase space which are mutual images under S [see Fig. 2(a)]. The period of these limit cycles is $T \approx 13.5$ s at $\rho = 1.72$ just above the bifurcation and grows with increasing ρ. As the light intensity increases, the radius of the limit cycles grows and at $\rho_1 \approx 1.808\,75$ the two limit cycles merge in a gluing bifurcation at the origin. At ρ_1 the limit cycles are homoclinic trajectories that leave the origin in the A_1, A_2 plane (very close to the A_1 axis) and return along the B_1 direction. Figure 2(b) shows this situation. Slightly above ρ_1 one has a single double-length limit cycle [Fig. 2(c)] which is symmetric under S. This is not a period-doubling bifurcation, however, as the homoclinic trajectories at ρ_1 have an infinite period.

At a certain intensity $\rho_1' > \rho_1$, the symmetric limit cycle loses stability and two asymmetric limit cycles are formed that are mutual images under S [Fig. 3(a)]. These merge in a second gluing bifurcation at $\rho_2 \approx 1.9474$, where the limit cycles are again homoclinic trajectories with an infinite period [Fig. 3(b)]. The symmetric quadruple-length limit cycle that is stable just above ρ_2 is shown in Fig. 3(c). This sequence of splitting and remerging of the limit cycle continues and the set of values ρ_i converge to a value $\rho_\infty \approx 1.98$. Beyond this point the motion is chaotic. The system exhibits typical signatures of low-dimensional deterministic chaos, such as great sensitivity to initial conditions and a positive Lyapunov exponent. The frequency spectrum of the mode amplitudes also shows this transition to chaos by changing

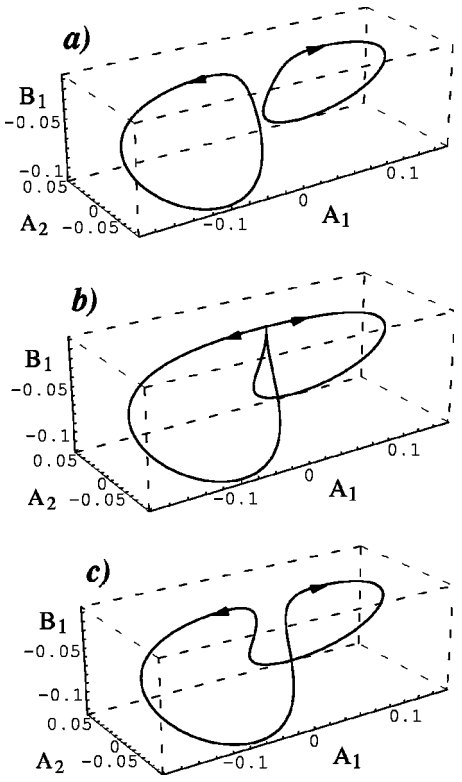

FIG. 2. (a) Simple limit cycles in three-dimensional phase space spanned by A_1, A_2, and B_1 at $s_0 = 7°$ and $\rho = 1.78$. (b) The limit cycle at $\rho = 1.808\,75$ at the first gluing bifurcation where it is composed of two homoclinic trajectories with infinite periods. (c) The double-length limit cycle at $\rho = 1.85$.

from a line spectrum (where all lines are integer multiples of the same fundamental frequency) to a continuous spectrum. We emphasize once more that, while this route to chaos involves the creation of *double-length* limit cycles at a sequence of points, it is very different from the usual period-doubling scheme, as the stable homoclinic limit cycle at the bifurcation has an infinite period. This quite distinct route to chaos was analyzed in a series of papers [11–13], but to our knowledge has never been observed in an experiment before.

Figure 4 shows the Lorenz-like strange attractor at $\rho = 2.18$. The evolution in phase space is organized around the three fixed points of the system; the origin (which became a saddle point at the primary instability at ρ_c) and the two fixed points formed in this primary instability that lost their stability in the secondary (Hopf) bifurcation at ρ_0. These points are so-called type II saddle foci—they are unstable foci in a plane and stable in a direction transverse to that plane. A trajectory spiraling outward from one saddle focus in its unstable plane will be attracted to the other saddle focus along that point's stable direction. Reaching the unstable plane of that fixed point, it begins spiraling outward, eventually being attracted back to the first saddle focus. The largest Lyapunov exponent at this intensity is $\lambda_L = 0.087\ \mathrm{s}^{-1}$.

At around $\rho = 2.5$ the Lorenz-like symmetric attractor gives way to two asymmetric attracting sets, again mutual images under S. They are of the form of a Möbius strip and the scenario is similar to that occuring in the Shimizu-Morioka model [13]. As the intensity is increased, the system

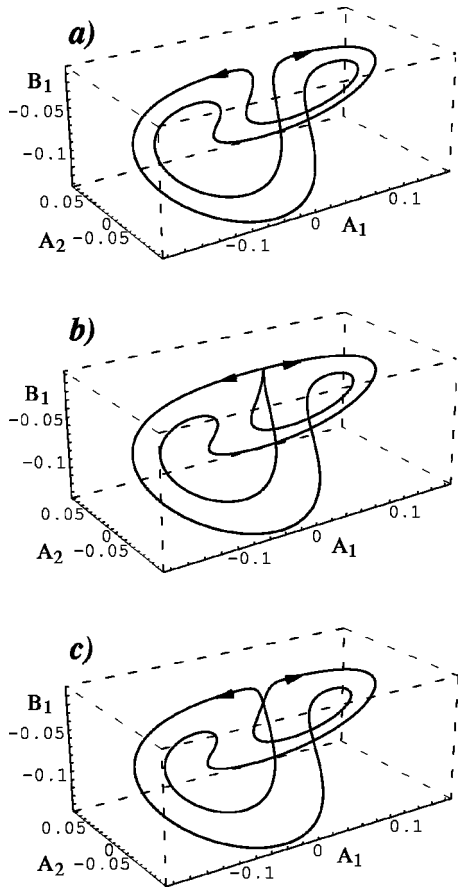

FIG. 3. (a) $\rho=1.94$, two asymmetric limit cycles that are mutual images under S. (b) The homoclinic limit cycles at the second gluing bifurcation at $\rho=1.9474$. (c) $\rho=1.96$, symmetric limit cycle created in the second gluing bifurcation.

returns to simple periodic behavior via an inverse period-doubling cascade.

A qualitative comparison of our simulations and the experimental observation shows that our model exhibits periodic oscillations and a transition to chaos just as observed in some of the experiments [6,8,9]. In these experiments periodic behavior is followed by a stochastic regime, after which the motion of the director is periodic again. This periodic behavior is followed by transition to chaos. In light of our model, this sequence can be interpreted as follows: The observation of the first periodic regime corresponds to the creation of limit cycles in the secondary Hopf bifurcation. As the intensity increases and the system nears the first gluing bifurcation, the limit cycles pass close to each other near the origin, and this makes it possible for the system to make random jumps between the limit cycles due to noise. Therefore a stochastic regime is observed in the vicinity of the gluing bifurcation. This is followed by periodic behavior again in the regime where the double-length limit cycle no longer passes very close to the origin [Fig. 2(c)]. This sequence of stochastic behavior in the vicinity of a gluing bifurcation followed by periodic behavior between two bifurcations should continue, but the intensity steps used in the experiments are too large to resolve any further bifurcations. Hence at higher intensities chaotic behavior was observed. The above interpretation is further supported by the observation of two modes of regular oscillation competing at a certain intensity value in [8,9], which could be the random jump between the two limit cycles close to the first gluing bifurcation.

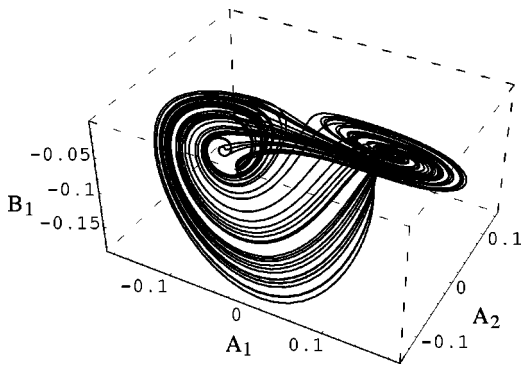

FIG. 4. Motion on the Lorenz-like strange attractor at $\rho=2.18$. The largest Lyapunov exponent of the attractor is $\lambda_L=0.087\ s^{-1}$.

A quantitative comparison is hampered by the fact that the spot size in the experiments is not larger than the width of the sample and one cannot assume the light to be a plane wave even in the middle of the beam, The threshold intensity of the onset of periodic behavior ($\rho=1.71$) is, however, quite near to the experimental values [6]. The system was observed to be already in the oscillatory regime at $\rho\approx1.86$ in [6], with the period of the oscillations being $T\approx12.5$ s. Our model exhibits sizable oscillations at $\rho=1.73$ with period $T\approx14$ s. The predicted increase of the period of the oscillations with ρ in the first oscillatory regime (before the first gluing bifurcation) is also in agreement with observations. The largest Lyapunov exponent of the attractor in the chaotic regime found in the experiments [7] ($0.1\pm0.015\ s^{-1}$) is consistent with that found in our simulations ($0.087\ s^{-1}$ at $\rho=2.18$).

B. Other routes to chaos

The scenario depicted above is not the only one to be exhibited by this sytem. This can be seen already from linear stability analysis of the basic state [10], which can be performed using the two modes A_1 and A_2 [see Eqs. (1)]. The analysis shows that the primary instability of the basic state is a stationary bifurcation only for small values of the phase shift κ and a Hopf bifurcation for larger values of κ (Fig. 5). (With given material parameters, κ is simply a quadratic function of the angle of incidence s_0.) The codimension-2 point (the Takens-Bogdanov point) where the linear part of the equations possesses a double zero eigenvalue is the point where the stationary primary instability that gives rise to two symmetry-degenerate fixed points becomes a Hopf instability that gives rise to a limit cycle. The secondary Hopf bifurcation that gives rise to two symmetry-degenerate limit cycles and the gluing bifurcation where these merge exist only below the Takens-Bogdanov point $\kappa_{TB}=2/\sqrt{13}$. For $\kappa>\kappa_{TB}$ there is only periodic oscillation of the director above a certain threshold intensity and there is no chaos. Slightly below κ_{TB} the series of gluing bifurcations does not continue to the accumulation point, the behavior returns to a simple limit cycle after a finite number of bifurcations. The number of these decreases as we approach κ_{TB}.

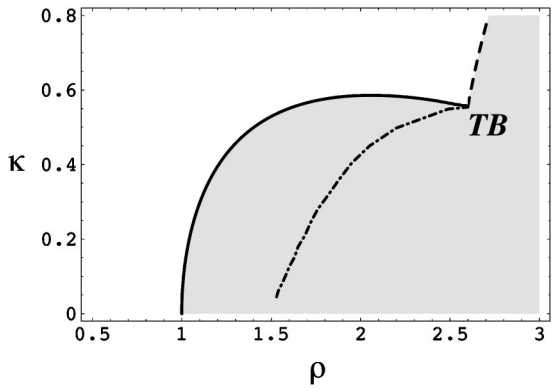

FIG. 5. Stability diagram of the homogeneous state on the ρ-κ plane. ρ is the dimensionless intensity parameter, $\kappa\pi$ is the phase shift between an ordinary and an extraordinary wave at $z=L$ in radians (see the text). In the region of instability (gray) the complex growth rate of perturbations has a positive real part. The line of stationary instability (solid line) joins the line of Hopf instability (dashed line) in the Takens-Bogdanov point ($\kappa_{\mathrm{TB}}=2/\sqrt{13}$, $\rho_{\mathrm{TB}}=13/5$). The line of secondary Hopf instability (dash-dotted line) also terminates at this point.

By varying the angle of incidence around 7° we find that the route the system takes to chaos changes as the light intensity increases. As an example, we will consider $s_0=4.5°$. The scenario is at first very similar to the case discussed previously. First a stationary reorientation takes place, then this state loses stability in a Hopf bifurcation, the resulting limit cycles merge in a gluing bifurcation, and after the creation of the asymmetric limit cycles there is a second gluing bifurcation that gives rise to a symmetric limit cycle just like the one shown in Fig. 3(c). After this, however, we have an inverse gluing bifurcation at $\rho\approx1.847$ that results in two asymmetric limit cycles again, which are mutual images under S. These asymmetric limit cycles then undergo a period-doubling cascade to produce two asymmetric strange attractors. As the intensity increases, the strange attractors widen and collide to merge into a symmetric strange attractor very similar to the one shown in Fig. 4. Figure 6 illustrates some steps in this sequence. The chaotic behavior is occasionally interrupted by periodic windows; a limit cycle that belongs to such a window is shown in Fig. 7. At still higher intensities, the system returns to simple periodic behavior.

The scenario is again very different at $s_0=3.5°$. Here we have observed the two routes to chaos to coexist. First there is a period doubling route to chaos as at $s_0=4.5°$, but then two homoclinic trajectories are created and coexist with the strange attractor. These homoclinic cycles then glue together and as the intensity is increased we again get a strange attractor [Fig. 8(a)] which coexists with the other strange attractor that was formed via the period-doubling cascade [Fig. 8(b)]. The existence of this latter is interrupted by a periodic window between $\rho=1.884$ and 1.888 [Fig. 8(c)]. At higher intensities the two strange attractors unite to form one very similar to that shown in Fig. 4.

Investigations with different angles and sample widths reveal that the system can exhibit a rich variety of different behaviors where gluing bifurcations, period-doubling bifurcations, chaotic attractors, and periodic windows alternate in various orders, and sometimes several attractors and limit cycles coexist at certain parameter values.

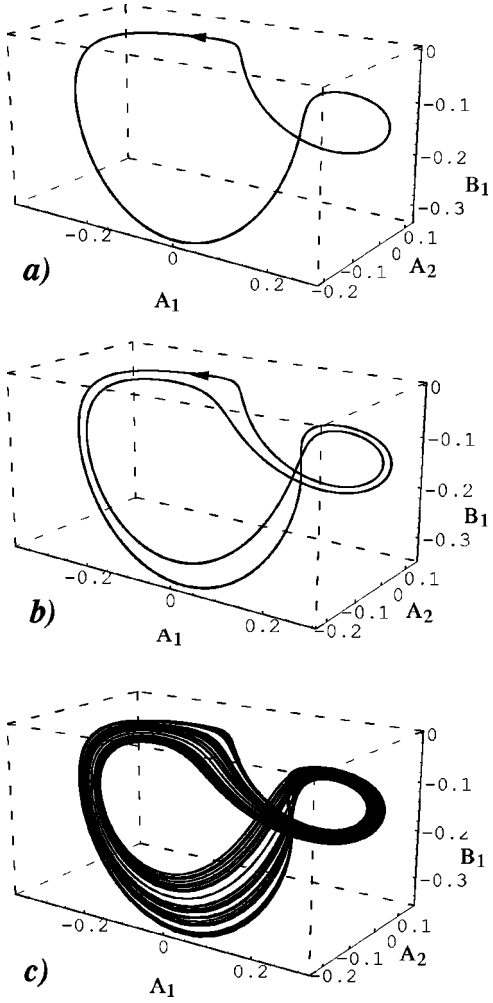

FIG. 6. (a) Asymmetric limit cycle at $s_0=4.5°$ and $\rho=1.85$. (b) Period-doubled asymmetric limit cycle at $\rho=1.88$. (c) Asymmetric strange attractor at $\rho=1.905$.

IV. REFINEMENTS OF THE MODEL

The fact that our model exhibits the scenario of transition to chaos via gluing bifurcations and agrees well with existing experimental observations is significant because it suggests that this scenario may be studied experimentally. However,

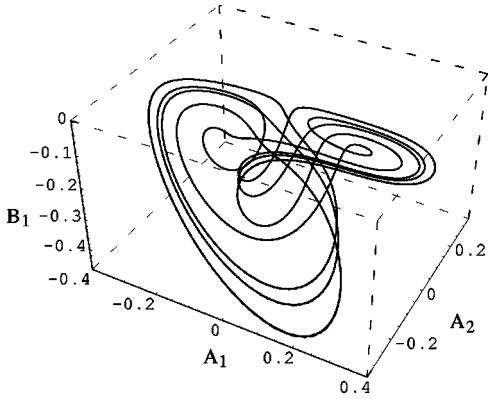

FIG. 7. Limit cycle in a periodic window at $s_0=4.5°$ and $\rho=2.1$.

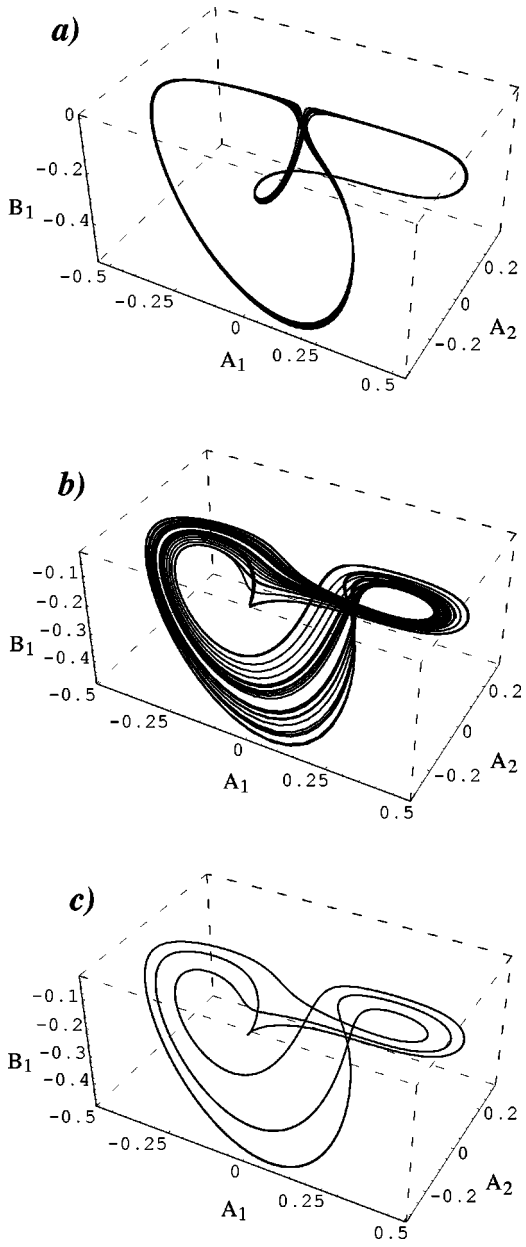

FIG. 8. (a) A strange attractor formed via gluing bifurcations and (b) one formed via period-doubling cascade that coexist at $s_0 = 3.5°$ and $\rho = 1.88$. (c) A periodic limit cycle that coexists with the strange attractor of (a) in the range $\rho = 1.884$–1.888.

our model can be further refined by adding more terms and/or higher-order nonlinearities. We can suggest that the gluing scenario may be experimentally observed on this physical system only if any such refined model can also exhibit the gluing scenario.

From previous work on this scenario of transition to chaos [11,12], we know that there are several necessary conditions for a set of dynamical equations to be able to exhibit the gluing scenario. First of all, there must exist a saddle point in phase space such that all but one of the eigenvalues of the Jacobian at this point have negative real parts. We denote the single postive eigenvalue by λ_1. Furthermore, the eigenvalue λ_2 with the second largest (least negative) real part must also be real. Second, the phase space $\Re$ must consist of two subspaces $\Re^s$ and $\Re^u$ with $\dim(\Re^s) \geqslant 2$ and $\dim(\Re^u) \geqslant 1$, and the set of equations must be invariant under the inversion of $\Re^s$ centered at the saddle point. The two eigenvalues λ_1 and λ_2 must belong to $\Re^s$ and $\Re^u$, respectively. Finally, we must have $\lambda_1 < -\lambda_2$ for the homoclinic cycles to be stable, which is also necessary for the observation of the gluing scenario.

It is not hard to see from the linear coefficients of our equations [Eqs. (1)] that around $\rho \approx 1$–2 all of these requirements are fulfilled. The saddle point is the origin where all amplitudes are zero and there is no reorientation of the LC. The symmetry property S of the equations is precisely the symmetry condition required, the two-dimensional subspace spanned by (A_1, A_2) corresponds to $\Re^s$, and the subspace of B_1 corresponds to $\Re^u$. The largest and only positive eigenvalue is close to L_{11}^A, with the corresponding eigenvector being in the A_1, A_2 plane and lying close to the A_1 direction. [The reason for this is that we assumed $\kappa^2 \ll 1$. Relaxing this condition does not change the fact that the eigenvector belongs to the (A_1, A_2) plane.] λ_2 is just $L_{11}^B = -1$. Around $\rho \approx 1$–2 we also have $\lambda_1 < -\lambda_2$.

It is easy to see that taking more modes into account does not change this situation. The symmetry S still fulfills our requirements, λ_2 remains the same, and only λ_1 will be perturbed slightly by the addition of further A_i modes. The corresponding eigenvector will also lie in the subspace spanned by the A's and close to the A_1 direction. Continuing the series expansions to higher order has no effect on the linear terms, so we can conclude that the above mentioned properties are retained by any refined model containing more modes and/or higher-order terms.

V. ADDITIONAL STATIC FIELDS

The precise values of the two largest eigenvalues λ_1, λ_2 also play an important role in the gluing bifurcation scenario. The so-called saddle index of the saddle point (here the origin) defined as $\nu = 1 + \lambda_2/\lambda_1$ (which must be negative for the homoclinic cycles to be stable) governs the asymptotic convergence rate of the series of bifurcation points ρ_n. This convergence rate is defined as

$$\delta(\nu) = \lim_{n \to \infty} \frac{\rho_n - \rho_{n-1}}{\rho_{n+1} - \rho_n} \tag{2}$$

and plays the same role as the famous Feigenbaum $\delta_F = 4.6692\ldots$ for the convergence rate of the period-doubling scenario. We mention that the famous Lorenz model exhibits the same symmetry properties as our system of equations, but there the saddle index is positive for the parameters where chaotic behavior develops. Thus the homoclinic orbits are unstable and chaos appears in a discontinuous manner.

We now consider slight extensions of our model with additional static electric or magnetic fields. One motivation for this is the role the linear eigenvalues at the origin play in determining the routes to chaos that this system may take. These eigenvalues, and hence the saddle index, depend on ρ and κ. The dependence on κ is weak, however, and since we consider only small angles of incidence we can vary ν only slightly using s_0. If we want to investigate how the transition to chaos with ρ depends on the saddle index, we may add some static fields to the system. It is easy to see that a homogeneous static field along any of the coordinate axis of

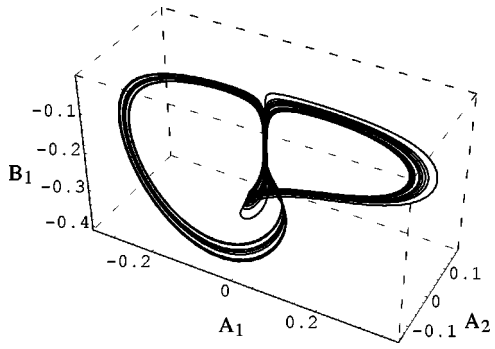

FIG. 9. Strange attractor in phase space at $s_0=7°$, $\eta=0.84$, and $\rho=0.8$.

Fig. 1. preserves the symmetry of the equations. These static fields introduce new linear terms and therefore the linear eigenvalues around the origin are changed. We can thus expect an even larger variety of nonlinear behavior to be observed, and the possibility arises of investigating how the route to chaos changes as the saddle index is varied.

As an example, we will consider adding a static electric field in the z direction, perpendicular to the plane of the cell. We will assume the static (low-frequency) dielectric anisotropy ε_a^{st} to be negative, which means that this additional field will help to destabilize the homogenous homeotropic alignment of the LC toward the x-y plane, i.e., help the director turn away from the z axis. (Assuming $\varepsilon_a>0$ for the light and $\varepsilon_a^{st}<0$ for the static field is by no means contradictory; the dielectric anisotropy in LCs is strongly frequency dependent and a number of materials fulfill these requirements.) The insertion of the effects of such a field into the equations is easily done and the linear coefficients can be written as

$$L^A_{mm}=-m^2+\eta+\rho+\frac{\kappa^2\rho}{m^2}[1+2(-1)^m],$$

$$L^A_{mn}=\frac{2(-1)^m\kappa^2\rho}{mn}, \quad m\neq n, \tag{3}$$

$$L^B_{mn}=-m^2\delta_{mn}+\eta,$$

where η is a dimensionless parameter that is proportional to the stength of the static electric field and is scaled such that the destabilization of the first mode due completely to the static field (the classical Fréedericksz transition) occurs at $\eta=1$. Using this new control parameter, one can change the value of the saddle index at a fixed value of the incidence angle and laser intensity.

Solution of the equations $\eta=0.1$ and $s_0=7°$ shows that the pure gluing scenario observed in the absence of the static electric field (see Sec. III A) changes into a mixed scenario where after the first two gluing bifurcations there is an inverse gluing bifurcation and then a period-doubling cascade. The new scenario is similar to the scenario at $s_0=4.5°$ without the static field (see Sec. III B). Investigations show that the gluing scenario is already replaced by the period-doubling cascade for small negative values of the saddle index, not just positive ones. If the magnitude of the static field is larger, the behavior of the system changes completely. An example is the strange attractor shown in Fig. 9, which can be observed at $s_0=7°$, $\eta=0.84$, and $\rho=0.8$.

Finally we mention that, as a practical advantage, one may use the additional static fields that help destabilize the homeotropic alignment of the LC to shift the region of interesting nonlinear behavior toward lower light intensities to facilitate the study of the system. This occurs, for example, if we add a stabilizing field in the y direction which helps the light field turn the director away from the z axis. [This corresponds to removing η from the third equation in Eq. (3).] In this case the nonlinear behavior is similar to the case of purely light-induced reorientation, but the threshold intensities are reduced.

VI. SUMMARY

We have studied theoretically the passage of a slightly oblique incidence plane wave through a homeotropically aligned nematic LC with the direction of polarization normal to the plane of incidence. We have derived a set of equations to describe the time-dependent director reorientation and found that at various intensities and angles of incidence the director can show complex nonlinear behavior. We have discovered that at certain parameter values the system diplays a route to chaos as yet unobserved in any experimental system. As predictions of our model agree well with existing experimental data, it seems likely that this distinct route to chaos could be experimentally realized in optically excited nematics in the geometry described. We have also shown that the properties of our model that make this route to chaos possible are robust against refinements of the model. Finally, we have shown that additional static fields may be used to generalize the system slightly and gain an even larger variety of interesting nonlinear behavior.

ACKNOWLEDGMENTS

The author wishes to thank L. Kramer, P. Coullet, and M. A. Zaks for helpful discussions. The author is also grateful to G. Cipparrone for having communicated new experimental results prior to publication. The hospitality of the Max Planck Institute for the Physics of Complex Systems in Dresden, Germany, where part of this research was carried out, is also gratefully acknowledged.

APPENDIX: DERIVATION OF EQUATIONS FOR THE REORIENTATION-MODE AMPLITUDES

To derive equations of motion for the time-dependent reorientation amplitudes we can use the equation for the director motion that can be derived from the usual orientational free energy, which includes the dielectric contribution averaged over the optical frequency oscillations [1,2],

$$F=\frac{K_1}{2}(\boldsymbol{\nabla}\cdot\mathbf{n})^2+\frac{K_2}{2}(\mathbf{n}\cdot\boldsymbol{\nabla}\times\mathbf{n})^2+\frac{K_3}{2}(\mathbf{n}\times\boldsymbol{\nabla}\times\mathbf{n})^2$$

$$-\frac{\varepsilon_a}{16\pi}|\mathbf{n}\cdot\mathbf{E}|^2. \tag{A1}$$

Here K_1,K_2,K_3 are the Frank constants of the LC and $\varepsilon_\perp$ is the (optical frequency) dielectric permittivity perpendicular to $\boldsymbol{n}$, $\varepsilon_a=\varepsilon_\parallel-\varepsilon_\perp$ the (optical frequency) dielectric anisot-

ropy. We consider solutions that depend on the z coordinate only. The equations of motion for the two angles $\varphi(z,t)$, $\theta(z,t)$ that describe the orientation of the director through

$$\mathbf{n}=(\sin\theta,\cos\theta\sin\varphi,\cos\theta\cos\varphi) \tag{A2}$$

[see Fig. 1(b)] can be deduced using standard variational procedures with the dissipation function $R=(\gamma/2)\dot{\mathbf{n}}^2$. Here γ is an effective rotational viscosity including the so-called backflow effects to lowest order (see, e.g., [17]). The calculations are lengthy, but straightforward. Assuming $[|\theta(z,t)|,|\varphi(z,t)|\ll 1]$, we can expand the expressions as a power series in the angles and neglect all terms that are fourth order or higher. When counting orders of magnitude, we must remember that the incident light is polarized initially along the y direction, and in the absence of director reorientation its polarization remains unchanged. The generation of E_x and E_z is therefore due to the reorientation and these components will be at least first order in the angles. To further simplify matters, we get rid of K_1 and K_2 by writing $K_1=2K_3/3$ and $K_2=K_3/2$, which approximately corresponds to the properties of the material $E7$ used in the experiments. With all these simplifications the equations of motion for the angles become

$$\begin{aligned}\gamma\partial_t\varphi=&K_3\partial_z^2\varphi\left(1-\frac{\varphi^2}{3}-\frac{\theta^2}{2}\right)+\frac{K_3}{6}\varphi\theta\partial_z^2\theta+\frac{2K_3}{3}\varphi(\partial_z\theta)^2\\&-3K_3\theta\partial_z\varphi\partial_z\theta-\frac{K_3}{3}\varphi(\partial_z\varphi)^2+\varepsilon_a|E_y|^2\left(\frac{\varphi}{8\pi}-\frac{\varphi^3}{12\pi}\right)\\&-\frac{\varepsilon_a\varphi}{8\pi}|E_z|^2+\varepsilon_a(E_z^*E_y+E_zE_y^*)\left(\frac{1}{16\pi}-\frac{\varphi^2}{8\pi}\right)\\&+\frac{\varepsilon_a\theta}{16\pi}(E_x^*E_y+E_xE_y^*)\end{aligned} \tag{A3a}$$

$$\begin{aligned}\gamma\partial_t\theta=&K_3\partial_z^2\theta\left(1-\frac{\theta^2}{3}-\frac{\varphi^2}{2}\right)+\frac{K_3}{6}\varphi\theta\partial_z^2\varphi+\frac{5K_3}{3}\theta(\partial_z\varphi)^2\\&-K_3\varphi\partial_z\varphi\partial_z\theta-\frac{K_3}{3}\theta(\partial_z\theta)^2+\frac{\varepsilon_a\theta}{8\pi}(|E_x|^2-|E_z|^2)\\&-\frac{\varepsilon_a\theta\varphi^2}{8\pi}|E_y|^2+\frac{\varepsilon_a}{16\pi}(E_x^*E_z+E_xE_z^*)\\&+\frac{\varepsilon_a\varphi}{16\pi}(E_x^*E_y+E_xE_y^*)-\frac{\varepsilon_a\varphi\theta}{8\pi}(E_y^*E_z+E_yE_z^*).\end{aligned} \tag{A3b}$$

The explicit t and z dependence of φ, θ, and E_i has been suppressed here for brevity. The main difficulty comes from the fact that the field components must be obtained from Maxwell's equations, which contain the ***n***-dependent dielectric tensor

$$\epsilon_{ij}(z,t)=\varepsilon_\perp\delta_{ij}+\varepsilon_a n_i n_j. \tag{A4}$$

Thus the field components will depend on the angles in a nontrivial way. We must find an expression for them correct to third order in the angles and insert it into Eqs. (A3a) and (A3b). Because we assumed only z dependence of the director, we can use the stratified medium approach for the wave propagation [2] and write the fields as $\mathbf{E}(\mathbf{r},t)=\frac{1}{2}[\mathbf{E}(z,t)e^{is_0k_0x}e^{-i\omega t}+\text{c.c.}]$, $\mathbf{H}(\mathbf{r},t)=1/2[\mathbf{H}(z,t)e^{is_0k_0x}e^{-i\omega t}+\text{c.c.}]$. ($k_0=\omega/c$ is the wave number in vacuum.) The slow time dependence of the functions $\mathbf{E}(z,t),\mathbf{H}(z,t)$ can be omitted in Maxwell's equations. We can also neglect the magnetic anisotropy at optical frequencies, so from the wave equations we get

$$\frac{d\bar{\Psi}}{dz}=ik_0\mathbf{D}\bar{\Psi}, \tag{A5}$$

where

$$\bar{\Psi}(z)=\begin{pmatrix}E_x(z)\\H_y(z)\\E_y(z)\\-H_x(z)\end{pmatrix} \tag{A6}$$

is a column vector with four elements and

$$\mathbf{D}(z)=\begin{pmatrix}-\frac{\epsilon_{xz}s_0}{\epsilon_{zz}} & 1-\frac{s_0^2}{\epsilon_{zz}} & -\frac{\epsilon_{yz}s_0}{\epsilon_{zz}} & 0\\ \epsilon_{xx}-\frac{\epsilon_{xz}^2}{\epsilon_{zz}} & -\frac{\epsilon_{xz}s_0}{\epsilon_{zz}} & \epsilon_{xy}-\frac{\epsilon_{xz}\epsilon_{yz}}{\epsilon_{zz}} & 0\\ 0 & 0 & 0 & 1\\ \epsilon_{xy}-\frac{\epsilon_{xz}\epsilon_{yz}}{\epsilon_{zz}} & -\frac{\epsilon_{yz}s_0}{\epsilon_{zz}} & \epsilon_{yy}-\frac{\epsilon_{yz}^2}{\epsilon_{zz}}-s_0^2 & 0\end{pmatrix}. \tag{A7}$$

The third component of the electric field is given by

$$E_z(z)=-\frac{s_0}{\epsilon_{zz}}H_y(z)-\frac{\epsilon_{xz}}{\epsilon_{zz}}E_x(z)-\frac{\epsilon_{yz}}{\epsilon_{zz}}E_y(z). \tag{A8}$$

To get an expression for $\mathbf{D}$ in terms of the angles we must substitute the expression for the director (A2) into Eq. (A4) and then the elements of the dielectric tensor into Eq. (A7). The complicated expression we get can be simplified by dropping all fourth and higher order terms with respect to the angles. We also introduce the notation $s=s_0/\sqrt{\varepsilon_\perp}$ (the angle of refraction of an ordinary wave in the absence of reorientation), and $\varepsilon_a'=\varepsilon_a/\varepsilon_\perp$ (anisotropy parameter). Furthermore, we split $\mathbf{D}$ into two parts; one contains the zeroth order terms (i.e., the part of $\mathbf{D}$ that belongs to the reorientationless state of the LC and is therefore not dependent on z) and the other contains the rest, $\mathbf{D}(z)=\mathbf{D}_0+\mathbf{D}_1(z)$:

$$\mathbf{D}_0=\begin{pmatrix} 0 & 1-\dfrac{s^2}{1+\varepsilon_a'} & 0 & 0 \\ \varepsilon_\perp & 0 & 0 & 0 \\ 0 & 0 & 0 & 1 \\ 0 & 0 & \varepsilon_\perp(1-s^2) & 0 \end{pmatrix}.$$

The nonzero elements of $\mathbf{D}_1$ are

$$(\mathbf{D}_1)_{11}=(\mathbf{D}_1)_{22}=-\frac{s\varepsilon_a'\sqrt{\varepsilon_\perp}\,\theta}{1+\varepsilon_a'}+\frac{s(2-\varepsilon_a')\varepsilon_a'\sqrt{\varepsilon_\perp}\,\theta^3}{3(1+\varepsilon_a')^2}+\frac{s(\varepsilon_a'-1)\varepsilon_a'\sqrt{\varepsilon_\perp}\,\theta\varphi^2}{2(1+\varepsilon_a')^2},$$

$$(\mathbf{D}_1)_{12}=-\frac{s^2\varepsilon_a'(\theta^2+\varphi^2)}{(1+\varepsilon_a')^2},$$

$$(\mathbf{D}_1)_{13}=(\mathbf{D}_1)_{42}=-\frac{s\varepsilon_a'\sqrt{\varepsilon_\perp}\,\varphi}{1+\varepsilon_a'}+\frac{s(2-\varepsilon_a')\varepsilon_a'\sqrt{\varepsilon_\perp}\,\varphi^3}{3(1+\varepsilon_a')^2}+\frac{s\varepsilon_a'\sqrt{\varepsilon_\perp}\,\theta^2\varphi}{(1+\varepsilon_a')^2},$$

$$(\mathbf{D}_1)_{21}=\frac{\varepsilon_a'\varepsilon_\perp\theta^2}{1+\varepsilon_a'},\quad (\mathbf{D}_1)_{23}=(\mathbf{D}_1)_{41}=\frac{\varepsilon_a'\varepsilon_\perp\theta\varphi}{1+\varepsilon_a'},$$

$$(\mathbf{D}_1)_{43}=\frac{\varepsilon_a'\varepsilon_\perp\varphi^2}{1+\varepsilon_a'}.$$

It is now convenient to use the formalism of Oldano [18] and transform to a representation where $\mathbf{D}_0$ is diagonal. To do this, we define the eigenvalues and eigenvectors: $\mathbf{D}_0\overline{\alpha_i}=a_i\overline{\alpha_i}$ where

$$a_1=-a_2=-\sqrt{\varepsilon_\perp}\sqrt{1-s^2},$$

$$a_3=-a_4=-\sqrt{\varepsilon_\perp}\sqrt{1-\frac{s^2}{1+\varepsilon_a'}},$$

and

$$\overline{\alpha}_{1,2}=\begin{pmatrix} 0 \\ 0 \\ \mp\dfrac{1}{\sqrt{\varepsilon_\perp}\sqrt{1-s^2}} \\ 1 \end{pmatrix},$$

$$\overline{\alpha}_{3,4}=\begin{pmatrix} \mp\dfrac{1}{\sqrt{\varepsilon_\perp}}\sqrt{1-\dfrac{s^2}{1+\varepsilon_a'}} \\ 1 \\ 0 \\ 0 \end{pmatrix}, \tag{A9}$$

and use the metric tensor

$$\mathbf{M}=\begin{pmatrix} 0 & 1 & 0 & 0 \\ 1 & 0 & 0 & 0 \\ 0 & 0 & 0 & 1 \\ 0 & 0 & 1 & 0 \end{pmatrix}$$

for the scalar product of these vectors. With this metric, the eigenvectors are orthogonal to one another, $\overline{\alpha_i^T}\mathbf{M}\overline{\alpha_j}=\delta_{ij}N_i$, with N_i being the ''norm'' of $\overline{\alpha_i}$ (which, however, can now be negative), and $\overline{\alpha_i^T}$ denotes a row vector. The identity $\Sigma_i(a_i/N_i)\overline{\alpha_i}\overline{\alpha_i^T}=\mathbf{D}_0$ can easily be proved. The eigenvectors and eigenvalues of $\mathbf{D}_0$ give the polarization and index of refraction of the four ''proper'' waves, i.e., waves that propagate without changing their state of polarization in the medium in the absence of director reorientation. There are two forward and two backward propagating modes, with the modes $\overline{\alpha_1},\overline{\alpha_2}$ being the ordinary waves and $\overline{\alpha_3},\overline{\alpha_4}$ being the extraordinary ones. From Eqs. (A6) and (A9) it is obvious that the ordinary waves have $E_y\neq 0$ and $E_x=H_y=0$, while the extraordinary waves have $E_y=0$ and $E_x\neq 0$, $H_y\neq 0$.

Writing the state vector in the form $\overline{\Psi}(z)=\Sigma b_k(z)\exp(ik_0a_kz)\overline{\alpha_k}$, we may transform Eq. (A5) into integral equations for the variables $b_k(z)$,

$$b_k(z)=b_k(0)+\int_0^z\frac{ik_0}{N_k}\sum P_{kj}(z')b_j(z')e^{-ik_0(a_k-a_j)z'}dz', \tag{A10}$$

where $P_{kj}(z)=\overline{\alpha_k^T}\mathbf{M}\mathbf{D}_1(z)\overline{\alpha_j}$ are the matrix elements of $\mathbf{D}_1$ between the eigenvectors. We expect the director orientation and the field components to change very little on the spatial scale of the light wavelength, so the functions b_j and P_{kj} will be almost constant on this scale, and the rapid oscillation of the exponential term in the integrand will average out those terms from the sum where the two eigenvalues a_k,a_j are of opposite sign. Thus modes traveling in opposite directions are not coupled by Eq. (A10). The physical meaning of this is that in the absence of dielectric boundaries (where the dielectric properties do change considerably on the spatial scale of the wavelength) there is no reflection.

As we have assumed strong anchoring at the boundaries, the initial condition $b_k(0)$ in Eq. (A10) in the present situation is a forward propagating ordinary wave at $z=0$ inside the medium. We therefore write $\mathbf{b}(0)=(0,A_0,0,0)$, the amplitude A_0 being proportional to the y component of the electric field at $z=0$. By virtue of the argument made in the previous paragraph (and neglecting reflection from the other boundary), we may drop the two backward propagating modes $\overline{\alpha_1}$ and $\overline{\alpha_3}$, as these will not play a role, and we may

reduce the problem to two variables. The four elements of the matrix P_{kj} that we will actually need, expressed to third order in the angles and with the coefficients of the various terms slightly simplified using $s^2 \ll 1$, are

$$P_{22}=\frac{\varepsilon_a' \varphi^2}{1+\varepsilon_a'},$$

$$P_{24}=P_{42}=-\frac{s\varepsilon_a'\varphi}{1+\varepsilon_a'}+\frac{\varepsilon_a'\theta\varphi}{1+\varepsilon_a'}+\frac{s\varepsilon_a'\theta^2\varphi}{(1+\varepsilon_a')^2}-\frac{s(-2+\varepsilon_a')\varepsilon_a'\varphi^3}{3(1+\varepsilon_a')^2},$$

$$P_{44}=-\frac{2s\varepsilon_a'\theta}{1+\varepsilon_a'}+\frac{\varepsilon_a'\theta^2}{1+\varepsilon_a'}-\frac{2s(-2+\varepsilon_a')\varepsilon_a'\theta^3}{3(1+\varepsilon_a')^2}-\frac{s^2\varepsilon_a'\varphi^2}{(1+\varepsilon_a')^2}-\frac{s(-1+\varepsilon_a')\varepsilon_a'\theta\varphi^2}{(1+\varepsilon_a')^2}.$$

The only expression appearing in the exponent within the integral in Eq. (A10) will be the difference of the two eigenvalues $k_0(a_2-a_4)$. We may expand this too as a power series in the small quantity s and drop those terms that do not cause a significant phase shift at the upper limit of the domain of integration L. Since $L \approx 10^2\lambda - 10^3\lambda$, one can see that with typical material parameters only the first term (which is quadratic in s) is needed and the second one (which is proportional to s^4) is not. Thus we define

$$\kappa=\frac{L}{\pi}k_0(a_4-a_2)\approx\frac{L}{\pi}\frac{s^2\varepsilon_a' k}{2(1+\varepsilon_a')},$$

the phase shift between the ordinary and extraordinary waves at the far edge of the layer ($z=L$) in the absence of reorientation divided by π. Here $k=k_0\sqrt{\varepsilon_\perp}$ is the wave vector in the medium. Introducing the scaled coordinate $g=z/L$, $g \in [0,1]$, we can now write Eq. (A10) for $b_2(g)$ and $b_4(g)$ as

$$b_2(g)=A_0+\frac{ik_0L}{N_2}\int_0^g [P_{22}(g')b_2(g') + P_{24}(g')b_4(g')e^{i\pi\kappa g'}]dg',$$

$$b_4(g)=\frac{ik_0L}{N_4}\int_0^g [P_{44}(g')b_4(g') + P_{42}(g')b_2(g')e^{-i\pi\kappa g'}]dg'. \qquad \text{(A11)}$$

This equation can be solved using successive iterations with $b_2^{(0)}=A_0$, $b_4^{(0)}=0$. To get the coefficients b_k to third order in the angles, we must iterate three times. The expressions will involve multiple integrals of the still unknown functions $\theta(g),\varphi(g)$ in a complicated way. They can be simplified slightly using $s^2 \ll 1$, and used to calculate the state vector, from which the fields can be obtained via Eqs. (A6) and (A8). These can then be used in Eqs. (A3a) and (A3b) to obtain an equation of motion for the angles. The equations can be simplified significantly if we restrict ourselves to the $\kappa^2 \ll 1$ case. Since using parameters that correspond to the experiments [6,7] gives us $\kappa^2 \sim 0.06$ (see [15]), we drop terms proportional to κ^4 or higher (there are no odd powers of κ in the expressions). In this case it is actually enough to iterate Eq. (A11) twice, because all terms that come from the third iteration are proportional to κ^4 or higher. It is also convenient to multiply Eqs. (A3a) and (A3b) by $L^2/K_3\pi^2$ and introduce the notation $\tau=\gamma L^2/\pi^2 K_3$ on the left hand side. The equations of motion now become

$$\tau\partial_t\varphi=\partial_g^2\varphi\frac{1}{\pi^2}\left(1-\frac{\varphi^2}{3}-\frac{\theta^2}{2}\right)+\frac{1}{6\pi^2}\varphi\theta\partial_g^2\theta+\frac{2}{3\pi^2}\varphi(\partial_g\theta)^2-\frac{3}{\pi^2}\theta\partial_g\varphi\partial_g\theta-\frac{1}{3\pi^2}\varphi(\partial_g\varphi)^2+\rho\varphi+\frac{\varepsilon_a'\rho\theta^2\varphi}{1+\varepsilon_a'}$$
$$+\frac{2(-1+2\varepsilon_a')\rho\varphi^3}{3(1+\varepsilon_a')}-\pi^2\kappa^2\rho[-\mathcal{L}^{(1)}(g\varphi)+g\mathcal{L}^{(1)}(\varphi)]+\frac{\pi^2\kappa^2\rho}{s}\{-\mathcal{L}^{(1)}(g\theta\varphi)+g\mathcal{L}^{(1)}(\theta\varphi)+2\mathcal{L}^{(2)}(\varphi,\theta)$$
$$+[-\mathcal{L}^{(1)}(g\varphi)+g\mathcal{L}^{(1)}(\varphi)]\theta\}+\frac{\pi^2\kappa^2\rho}{s^2}\{-2\mathcal{L}^{(2)}(\varphi,\theta)\theta-\mathcal{L}^{(2)}(\varphi,\theta^2)-2\mathcal{L}^{(2)}(\varphi\theta,\theta)$$
$$+[\mathcal{L}^{(1)}(g\varphi\theta)-g\mathcal{L}^{(1)}(\varphi\theta)]\theta+\mathcal{L}^{(1)}(\varphi)\mathcal{L}^{(1)}(\varphi^2)-2\mathcal{L}^{(2)}(\varphi,\varphi)\varphi-\mathcal{L}^{(2)}(\varphi^2,\varphi)\}, \qquad \text{(A12a)}$$

$$\tau\partial_t\theta=\partial_g^2\theta\frac{1}{\pi^2}\left(1-\frac{\theta^2}{3}-\frac{\varphi^2}{2}\right)+\frac{1}{6\pi^2}\varphi\theta\partial_g^2\varphi+\frac{5}{3\pi^2}\theta(\partial_g\varphi)^2-\frac{1}{\pi^2}\varphi\partial_g\varphi\partial_g\theta-\frac{1}{3\pi^2}\theta(\partial_g\theta)^2-\frac{\rho\theta\varphi^2}{1+\varepsilon_a'}+\frac{\pi^2\kappa^2\rho}{s}$$
$$\times\{-\mathcal{L}^{(1)}(\varphi)^2+[-\mathcal{L}^{(1)}(g\varphi)+g\mathcal{L}^{(1)}(\varphi)]\varphi\}+\frac{\pi^2\kappa^2\rho}{s^2}\{2\mathcal{L}^{(1)}(\theta\varphi)\mathcal{L}^{(1)}(\varphi)+\mathcal{L}^{(1)}(\varphi)^2\theta$$
$$+[\mathcal{L}^{(1)}(g\theta\varphi)-g\mathcal{L}^{(1)}(\theta\varphi)]\varphi-2\mathcal{L}^{(2)}(\varphi,\theta)\varphi\}, \qquad \text{(A12b)}$$

where we have introduced the two integral operators

$$\mathcal{L}^{(1)}(x(g))=\int_0^g x(g')dg', \quad \mathcal{L}^{(2)}(x(g),y(g))=\int_0^g y(g')\int_0^{g'} x(g'')dg''dg' \qquad \text{(A13)}$$

that operate upon functions of the scaled length g. At this point it is straightforward to write the angles as a series of sine functions $\varphi(g,t)=\Sigma_n A_n(t)\sin(n\pi g)$, $\theta(g,t)=\Sigma_n B_n(t)\sin(n\pi g)$, carry out the integrations, and project the result on the various modes to get a set of nonlinear ODE's for the mode amplitudes. For the minimal model of three variables $\{A_1,A_2,B_1\}$ these equations become

$$\tau\dot{A}_1(t)=A_1(t)(-1-\kappa^2\rho+\rho)-A_2(t)\kappa^2\rho+A_1(t)B_1(t)\frac{\pi\kappa^2\rho}{s}+A_2(t)B_1(t)\frac{(256+9\pi^2)\kappa^2\rho}{36s\pi}$$
$$+A_1(t)B_1(t)^2\left(-\frac{1}{3}+\frac{3\varepsilon_a'\rho}{4(1+\varepsilon_a')}-\frac{(141+4\pi^2)\kappa^2\rho}{48s^2}\right)+A_1(t)^3\frac{1}{6}\left(1-\frac{3(-2\varepsilon_a'+1)\rho}{(1+\varepsilon_a')}-\frac{3\kappa^2\rho}{s^2}\right)-A_2(t)B_1(t)^2\frac{127\kappa^2\rho}{36s^2}$$
$$+A_1(t)A_2(t)^2\left(\frac{5}{6}+\frac{(2\varepsilon_a'-1)\rho}{(1+\varepsilon_a')}+\frac{7\kappa^2\rho}{8s^2}\right)+A_1(t)^2A_2(t)\frac{\kappa^2\rho}{4s^2}+A_2(t)^3\frac{\kappa^2\rho}{2s^2}, \tag{A14a}$$

$$\tau\dot{A}_2(t)=A_2(t)\left(-4+\frac{3\kappa^2\rho}{4}+\rho\right)+A_1(t)\kappa^2\rho-A_1(t)B_1(t)\frac{(256+9\pi^2)\kappa^2\rho}{36s\pi}-A_2(t)B_1(t)\frac{64\kappa^2\rho}{9s\pi}$$
$$+A_2(t)B_1(t)^2\left(\frac{5}{4}+\frac{\varepsilon_a'\rho}{2(1+\varepsilon_a')}+\frac{185\kappa^2\rho}{72s^2}\right)+A_1(t)B_1(t)^2\frac{127\kappa^2\rho}{36s^2}+A_1(t)^2A_2(t)\left(\frac{5}{6}+\frac{(2\varepsilon_a'-1)\rho}{(1+\varepsilon_a')}-\frac{9\kappa^2\rho}{8s^2}\right)$$
$$+A_2(t)^3\left(\frac{2}{3}-\frac{(-2\varepsilon_a'+1)\rho}{2(1+\varepsilon_a')}-\frac{5\kappa^2\rho}{8s^2}\right)+A_1(t)^3\frac{\kappa^2\rho}{4s^2}-A_1(t)A_2(t)^2\frac{3\kappa^2\rho}{2s^2}, \tag{A14b}$$

$$\tau\dot{B}_1(t)=-B_1(t)+A_1(t)^2\frac{(-16+\pi^2)\kappa^2\rho}{2s\pi}-A_2(t)^2\frac{32\kappa^2\rho}{9s\pi}+A_1(t)A_2(t)\frac{(-256+9\pi^2)\kappa^2\rho}{36s\pi}$$
$$+A_1(t)^2B_1(t)\frac{1}{48}\left(20-\frac{36\rho}{1+\varepsilon_a'}+\frac{(147-4\pi^2)\kappa^2\rho}{s^2}\right)+\frac{B_1(t)^3}{6}+A_2(t)^2B_1(t)\left(\frac{13}{4}-\frac{\rho}{2(1+\varepsilon_a')}+\frac{185\kappa^2\rho}{72s^2}\right)$$
$$+A_1(t)A_2(t)B_1(t)\frac{7\kappa^2\rho}{2s^2}. \tag{A14c}$$

[1] N. V. Tabiryan, A. V. Sukhov, and B. Ya. Zel'dovich, Mol. Cryst. Liq. Cryst. **136**, 1 (1985).

[2] F. Simoni, *Nonlinear Optical Properties of Liquid Crystals* (World Scientific, Singapore, 1997).

[3] E. Santamato, B. Daino, M. Romagnoli, M. Settembre, and Y. R. Shen, Phys. Rev. Lett. **57**, 2423 (1986); E. Santamato, G. Abbate, P. Maddalena, L. Marrucci, and Y. R. Shen, *ibid.* **64**, 1377 (1990).

[4] B. Ya. Zel'dovich, S. K. Merzlikin, N. F. Pilipetskii, A. V. Sukhov, and N. V. Tabiryan, Pis'ma Zh. Éksp. Teor. Fiz. **37**, 568 (1983) [JETP Lett. **37**, 676 (1983)].

[5] A. S. Zolot'ko, V. F. Kitaeva, N. Kroo, N. N. Sobolev, A. P. Sukhorukov, V. A. Troshkin, and L. Czillag, Zh. Éksp. Teor. Fiz. **87**, 859 (1984) [Sov. Phys. JETP **60**, 488 (1984)]; V. F. Kitaeva, N. Kroo, N. N. Sobolev, A. P. Sukhorukov, V. Yu. Fedorovich, and L. Czillag, *ibid.* **62**, 520 (1985).

[6] G. Cipparrone, V. Carbone, C. Versace, C. Umeton, R. Bartolino, and F. Simoni, Phys. Rev. E **47**, 3741 (1993).

[7] V. Carbone, G. Cipparrone, C. Versace, C. Umeton, and R. Bartolino, Mol. Cryst. Liq. Cryst. Sci. Technol., Sect. A **251**, 167 (1994); Phys. Rev. E **54**, 6948 (1996); C. Versace, V. Carbone, G. Cipparrone, C. Umeton, and R. Bartolino, Mol. Cryst. Liq. Cryst. Sci. Technol., Sect. A **290**, 267 (1996).

[8] A. S. Zolotko *et al.*, Liq. Cryst. **15**, 787 (1993).

[9] G. Cipparrone, G. Russo, V. Carbone, G. Strangi, V. Carbone, Opt. Commun. **173**, 1 (2000).

[10] N. V. Tabiryan, A. L. Tabiryan-Murazyan, V. Carbone, G. Cipparrone, C. Umeton, and C. Versace, Opt. Commun. **154**, 70 (1998).

[11] A. Arneodo, P. Coullet, and C. Tresser, Phys. Lett. **81A**, 197 (1981); Y. Kuramoto and S. Koga, *ibid.* **92A**, 1 (1982).

[12] D. V. Lyubimov and M. A. Zaks, Physica D **9**, 52 (1983).

[13] A. L. Shil'nikov, Physica D **62**, 338 (1993).

[14] G. Demeter and L. Kramer, Phys. Rev. Lett. **83**, 4744 (1999).

[15] The parameters that correspond to the experimental setup [6,7] are $L=50$ μm, $\lambda=514.5$ nm, $s_0=7°$. For the parameters of the chemical E7 used we took for the ratios of the Frank constants $K_1/K_3=2/3$ (British Drug House data sheet) and $K_2/K_3=1/2$ (our estimate). The ratio K_3/γ was taken to be 10^{-6} cm^2/s from a direct measurement in the same geometry [16]. This value should already include the backflow effects. For the dielectric constants at optical frequency we took $\varepsilon_\perp=2.25$ and $\varepsilon_a=0.76$ from [10].

[16] G. Cipparrone, D. Duca, C. Versace, C. Umeton, and N. V. Tabiryan, Mol. Cryst. Liq. Cryst. Sci. Technol., Sect. A **266**, 263 (1995).

[17] E. Guyon, R. Meyer, and J. Salan, Mol. Cryst. Liq. Cryst. **54**, 261 (1979).

[18] C. Oldano, Phys. Rev. A **40**, 6014 (1989).